Regular Article – Experimental Physics

# Neutron-induced fission cross-section of $^{233}$U in the energy range $0.5 < E_n < 20\,\text{MeV}$

The n_TOF Collaboration

F. Belloni[1], M. Calviani[2,3], N. Colonna[4], P. Mastinu[2], P.M. Milazzo[1,a], U. Abbondanno[1], G. Aerts[5], H. Álvarez[6], F. Alvarez-Velarde[7], S. Andriamonje[5], J. Andrzejewski[8], L. Audouin[9], G. Badurek[10], P. Baumann[11], F. Bečvář[12], E. Berthoumieux[5], F. Calviño[13], D. Cano-Ott[6], R. Capote[14,15], C. Carrapiço[16], P. Cennini[3], V. Chepel[17], E. Chiaveri[3], G. Cortes[13], A. Couture[18], J. Cox[18], M. Dahlfors[3], S. David[11], I. Dillmann[9], C. Domingo-Pardo[19], W. Dridi[5], I. Duran[6], C. Eleftheriadis[20], M. Embid-Segura[6], A. Ferrari[3], R. Ferreira-Marques[17], K. Fujii[1], W. Furman[21], I. Goncalves[16], E. Gonzalez-Romero[6], A. Goverdovski[22], F. Gramegna[2], C. Guerrero[7], F. Gunsing[5], B. Haas[23], R. Haight[24], M. Heil[9], A. Herrera-Martinez[3], M. Igashira[25], E. Jericha[10], F. Käppeler[9], Y. Kadi[3], D. Karadimos[26], D. Karamanis[26], M. Kerveno[11], P. Koehler[27], E. Kossionides[28], M. Krtička[12], C. Lamboudis[20], H. Leeb[10], A. Lindote[17], I. Lopes[17], M. Lozano[29], S. Lukic[11], J. Marganiec[8], S. Marrone[4], T. Martínez[7], C. Massimi[30], M.H. Meaze[4], A. Mengoni[3,14], C. Moreau[1], M. Mosconi[9], F. Neves[17], H. Oberhummer[10], S. O'Brien[18], J. Pancin[5], C. Papachristodoulou[26], C. Papadopoulos[31], C. Paradela[6], N. Patronis[26], A. Pavlik[32], P. Pavlopoulos[33], L. Perrot[5], M.T. Pigni[10], R. Plag[9], A. Plompen[34], A. Plukis[5], A. Poch[13], J. Praena[29], C. Pretel[13], J. Quesada[29], T. Rauscher[35], R. Reifarth[24], M. Rosetti[36], C. Rubbia[37], G. Rudolf[11], P. Rullhusen[34], J. Salgado[16], C. Santos[16], L. Sarchiapone[3], I. Savvidis[20], C. Stephan[38], G. Tagliente[4], J.L. Tain[19], L. Tassan-Got[38], L. Tavora[16], R. Terlizzi[4], G. Vannini[30], P. Vaz[16], A. Ventura[36], D. Villamarin[7], M.C. Vincente[7], V. Vlachoudis[3], R. Vlastou[31], F. Voss[9], S. Walter[9], M. Wiescher[18], and K. Wisshak[9]

1 Istituto Nazionale di Fisica Nucleare (INFN), Trieste, Italy
2 Istituto Nazionale di Fisica Nucleare (INFN), Laboratori Nazionali di Legnaro, Italy
3 CERN, Geneva, Switzerland
4 Istituto Nazionale di Fisica Nucleare (INFN), Bari, Italy
5 CEA, Irfu, Gif-sur-Yvette, France
6 Universidade de Santiago de Compostela, Spain
7 Centro de Investigaciones Energeticas Medioambientales y Technologicas, Madrid, Spain
8 University of Lodz, Lodz, Poland
9 Karlsruhe Institute of Technology, Campus Nord, Institut für Kernphysik, Germany
10 Atominstitut der Österreichischen Universitäten, Technische Universität Wien, Austria
11 Centre National de la Recherche Scientifique/IN2P3 - IReS, Strasbourg, France
12 Faculty of Mathematics and Physics, Charles University in Prague, Czech Republic
13 Universitat Politecnica de Catalunya, Barcelona, Spain
14 International Atomic Energy Agency (IAEA), NAPC/Nuclear Data Section, Vienna, Austria
15 Universidad de Sevilla, Spain
16 Instituto Tecnológico e Nuclear (ITN), Lisbon, Portugal
17 LIP - Coimbra and Departamento de Fisica da Universidade de Coimbra, Portugal
18 University of Notre Dame, Notre Dame, IN, USA
19 Instituto de Física Corpuscular, CSIC-Universidad de Valencia, Spain
20 Aristotle University of Thessaloniki, Greece
21 Joint Institute for Nuclear Research, Frank Laboratory of Neutron Physics, Dubna, Russia
22 Institute of Physics and Power Engineering, Obninsk, Russia
23 Centre National de la Recherche Scientifique/IN2P3 - CENBG, Bordeaux, France
24 Los Alamos National Laboratory, Los Alamos, NM, USA

a e-mail: paolo.milazzo@ts.infn.it

[25] Tokyo Institute of Technology, Tokyo, Japan
[26] University of Ioannina, Greece
[27] Oak Ridge National Laboratory, Physics Division, Oak Ridge, TN, USA
[28] NCSR, Athens, Greece
[29] Universidad de Sevilla, Spain
[30] Dipartimento di Fisica, Università di Bologna and Sezione INFN di Bologna, Italy
[31] National Technical University of Athens, Greece
[32] Institut für Fakultät für Physik, Universität Wien, Austria
[33] Pôle Universitaire Léonard de Vinci, Paris La Défense, France
[34] CEC-JRC-IRMM, Geel, Belgium
[35] Department of Physics and Astronomy, University of Basel, Switzerland
[36] ENEA, Bologna, Italy
[37] Università degli Studi di Pavia, Pavia, Italy
[38] Centre National de la Recherche Scientifique/IN2P3 - IPN, Orsay, France

**Abstract.** The neutron-induced fission cross-section of $^{233}$U has been measured at the CERN n_TOF facility relative to the standard fission cross-section of $^{235}$U between 0.5 and 20 MeV. The experiment was performed with a fast ionization chamber for the detection of the fission fragments and to discriminate against $\alpha$-particles from the natural radioactivity of the samples. The high instantaneous flux and the low background of the n_TOF facility result in data with uncertainties of $\approx 3\%$, which were found in good agreement with previous experiments. The high quality of the present results allows to improve the evaluation of the $^{233}$U(n,f) cross-section and, consequently, the design of energy systems based on the Th/U cycle.

# 1 Introduction

To reduce the emissions responsible of the greenhouse effect is nowadays a mandatory objective. Nuclear energy, in conjunction with renewable sources, is a viable option. On the other hand, current estimates [1] predict that the uranium resources will be exhausted within 80 years given the present exploitation rate and the incomplete usage by conventional reactors. This limit could be significantly delayed (hundreds of years [1]) by the design of systems based on alternative fuel cycles [2], of sub-critical Accelerator-Driven Systems (ADS) [3–5], and of advanced Generation-IV reactors [6]. In particular, one of the most promising concepts would be the use of the Th/U fuel cycle, where the fissile isotope $^{233}$U is produced by neutron capture on $^{232}$Th and subsequent $\beta$-decay.

The Th/U fuel cycle has attractive features, because thorium is three times more abundant than uranium and it consists mainly of $^{232}$Th. Furthermore, the production of transuranium actinides is strongly reduced, thus minimizing the problem of disposing high level nuclear wastes, while the breeding reaction presents practically no proliferation risk. Finally, it should be considered that this cycle can be implemented in thermal breeding reactors (thus simplifying safety issues) as well as in sub-critical accelerator-driven systems.

The development of advanced reactors based on new fuel cycles requires a strong effort for improving the basic nuclear data involved in reactor physics, including a better accuracy of neutron-induced fission cross-sections. In particular, the design of systems based on the Th/U fuel cycle depends on a better determination of the $^{233}$U$(n, f)$ cross-section.

Existing experimental data come from few measurements [7–14], with only two of them relatively recent [12, 14], which show discrepancies of up to 10%. The purity of the sample, the detector response to the related $\alpha$ activity, the knowledge of the detection efficiency, of the neutron flux and beam profile are some of the possible sources of systematic errors affecting previous results.

The measurement at the CERN n_TOF facility aims at reducing the uncertainty of the main reaction in the Th/U fuel cycle, taking advantage of the favorable properties of this installation, where the very high instantaneous neutron flux and extremely low duty cycle allows one to minimize the background related to the $\alpha$ activity of the sample. Systematic uncertainties associated with detection efficiency, dead-time effects, and signal pile-up could be further reduced by a special experimental setup and a data acquisition system based on fast digitizers. All these features have already been exploited by the n_TOF Collaboration in a comprehensive program for measurements of neutron capture and fission cross-sections, which is intended to contribute to an improvement of evaluated databases [15]. In this context, first results on the neutron-induced fission cross-section of $^{233}$U from thermal to 1 MeV have recently been published [16].

The present work focuses on the fission cross-section of $^{233}$U in the energy region from 0.5 to 20 MeV. The experimental details are presented in sect. 2, while the data analysis procedure is described in sect. 3. The extracted cross-section is presented and compared with previous measurements and current evaluations in sect. 4. Conclusions are drawn in sect. 5.

# 2 Measurement

## 2.1 The n_TOF facility

The measurement was performed at CERN using the pulsed neutron beam of the n_TOF facility, which is generated by proton-induced spallation reactions on a massive lead target [17]. The main characteristics of the proton beam are its high energy ($E_p = 20$ GeV), high intensity ($I_p = 7 \times 10^{12}$ protons per bunch), short pulse width ($\Delta t = 6$ ns), and low duty factor. The low pulse repetition rate of 0.4 Hz and the favorable background conditions in the experimental area make this facility unique for high-resolution time-of-flight (TOF) measurements of neutron-induced reaction cross-sections [18]. Moreover, the high instantaneous flux of $10^5$ neutrons/cm$^2$/pulse at the sample position strongly reduces the background induced by the natural radioactivity of the samples.

The spallation neutrons are slowed down in the lead target and moderated in a 5.8 cm thick layer of cooling water surrounding the target. The experimental area at a distance of 187 m is connected with the target by an evacuated flight path with two collimators at 137 and 176 m. The aperture of the second collimator, which is 8 cm in diameter, defines the spatial profile of the neutron beam used in the fission measurements. The beam line extends 12 m beyond the experimental area to minimize the effect of back-scattered neutrons. Background due to fast charged particles is suppressed by a 1.5 T sweeping magnet, heavy concrete walls, and a 3.5 m thick iron shielding located along the beam line [18].

## 2.2 The experimental setup

The measurement has been carried out with a fast ionization chamber (FIC) [19] built in collaboration between the Joint Institute of Nuclear Research (JINR, Dubna, Russian Federation), the Institute of Physics and Power Engineering (IPPE, Obninsk, Russian Federation), the Istituto Nazionale di Fisica Nucleare (INFN), and CERN. The setup consists of a stack of ionization chambers, thus allowing the simultaneous measurement on several isotopes. Each chamber consists of a central Al cathode 100 $\mu$m in thickness plated on both sides with sample material, and two 15 $\mu$m thick Al anodes at a distance of 5 mm from the cathode to define the electric field. The electrodes are 12 cm in diameter, while the sample deposit itself is 8 cm in diameter to match the size of the neutron beam. The detector setup is operated with a gas mixture of 90% Ar and 10% CF$_4$ at a pressure of 720 mbar.

Fission events were detected via the energy deposited in the gas by the fission fragments produced in very thin layers of fissile material. The total masses of the samples

**Table 1.** Total sample masses used in the $^{233}$U$(n, f)$ measurement; the $^{235}$U sample has been used as reference.

| Sample | Chemical form | Mass (mg) | Activity (kBq) |
|--------|---------------|-----------|----------------|
| $^{233}$U | $U_3O_8$ | 30.8 | 5530 |
| $^{235}$U | $U_3O_8$ | 31.8 | 0.2 |

used in the present measurement are reported in table 1 ($^{235}$U was used as reference) together with their $\alpha$ activities. The samples were prepared by means of the painting technique, using almost isotopically pure materials with $^{233}$U and $^{235}$U enrichments of 99.0% (small admixtures of $^{234}$U (0.74%), $^{235}$U (0.23%), and $^{238}$U (0.04%) are present) and 99.992%, respectively.

The neutron TOF was determined as the difference between the prompt signal generated by $\gamma$-rays and relativistic particles produced in interactions of the proton beam in the spallation and the detected fission events, respectively. The absence of a Frisch grid in the fission chambers and optimized front-end electronics resulted in a fast signal with good timing properties, *i.e.* 50 ns rise and 120 ns decay time. All signals were recorded with fast digitizers with a sampling rate of 100 MSamples/s using the standard n_TOF data acquisition system [20] and stored in the central data recording system of CERN from where they can be retrieved for off-line analysis.

## 3 Data analysis

The first step of the analysis consisted of the off-line determination of the TOF and of the energy deposited in the detector by each fission event. In order to extract the neutron energy, the TOF-energy relation with the calibration of ref. [21] was used, which takes the neutron production mechanism in the spallation target and the subsequent moderation process [18] into account. The length of the flight path was obtained by means of a careful analysis of the well-known $^{235}$U resonances [21].

The prompt $\gamma$-flash from spallation reactions in the Pb target is so intense that it produces strong oscillations of the detector baseline, which last for several microseconds and exceed the fission signals due to neutrons above a few MeV in energy. This problem has been overcome by observing that the $\gamma$-flashs in adjacent electrodes exhibit identical patterns. Therefore, the fission signals could be recovered by the software compensation technique described in ref. [22].

The experimental pulse height was compared with detailed Monte Carlo simulations with the FLUKA code [23] to describe the energy losses of $\alpha$-particles and fission fragments in the gas volume and in the sample layers. The kinetic energy and mass of the fission fragments were randomly generated according to the respective distributions [24,25]. The result of the simulation for the $^{233}$U sample in fig. 1 shows that the $\alpha$ background is well separated from the fission fragments distribution and that both components are well characterized.
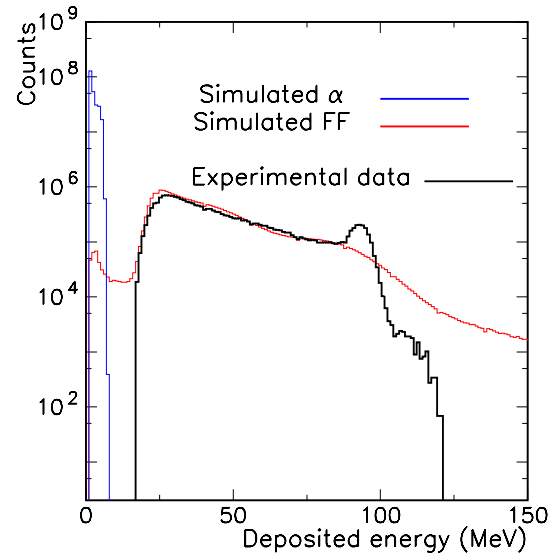


**Fig. 1.** Comparison between the measured pulse height distribution (thick black line) and the simulated spectrum indicating the $\alpha$-particle background at low energies and the response to fission fragments (thin blue and red lines). The difference between measurement and simulation is due to saturation effects in the detector above 80 MeV. The measured part is truncated at $\approx 16$ MeV corresponding to the threshold adopted in the analysis.

The black histogram in fig. 1 shows the experimental pulse height spectrum for $^{233}$U averaged over the neutron energy range between 0.5 and 20 MeV. The comparison with the simulation confirms that the $\alpha$ background can be almost completely discriminated by the energy threshold of about 16 MeV, whereas only a very small fraction of the fission fragments falls below that threshold. The differences between the measured and simulated distributions at the highest energies are due to saturation effects in the recorded signals.

The $^{233}$U$(n, f)$ cross-section has been extracted relative to the $^{235}$U$(n, f)$ cross-section, which is a well-established standard in the neutron energy range from 0.15 eV to 200 MeV [26],

$$\sigma_{233}(n,f) = c \cdot \sigma_{235}(n,f) \cdot \frac{N_{233}}{N_{235}} \cdot \frac{m_{235}}{m_{233}} \cdot \frac{A_{233}}{A_{235}}, \quad (1)$$

where $c$ is a correction factor, that combines the detection efficiencies and dead-time effects, and $\sigma_{235}(n,f)$ is the tabulated ENDF/B-VII.0 cross-section [15]. $N_{23x}$ denotes the number of detected fission events, $m_{23x}$ the sample mass for the $^{23x}$U isotope, and $A_{23x}$ the atomic mass of isotope $^{23x}$U.

The ratio method can be applied in this case because both samples were exposed to the same neutron flux and were measured with very similar detectors showing nearly identical efficiencies and signal shapes. Compared to a direct measurement, the ratio method allows one to minimize also the systematic uncertainties related to the determination of the neutron flux.

Remaining differences between the $^{233}$U and the reference sample are due to the sample thickness, which affects the detection efficiency, and to the count rate, which leads to slightly different dead-time and pile-up corrections. Although only of the order of a few percent, these differences have been carefully evaluated. The sample-related corrections are expressed as

$$c = \frac{\varepsilon_{235} \cdot d_{235}}{\varepsilon_{233} \cdot d_{233}}, \qquad (2)$$

where $\varepsilon$ represents the efficiency for the detection of fission fragments and $d$ the loss of counts due to dead-time and pile-up.

The detection efficiency depends essentially on the sample thickness and on the 16 MeV threshold for the pulse height distribution. From the Monte Carlo simulations described above, the efficiencies were found to be 97.7% and 95.1% for $^{233}$U and $^{235}$U, resulting in an efficiency correction of 2.6%.

Although dead-time problems are minimized with data acquisition system based on flash ADCs [20], a small effect persists because of the 270 ns resolving time in the signal reconstruction routine. The related corrections have been evaluated by means of a non-paralyzable model, where the instantaneous count rate was determined for each sample as a function of the neutron energy. The dead-time correction was found to increase with neutron energy from 1% at 1 MeV to 3.8% at 20 MeV.

### 3.1 Discussion of uncertainties

The overall uncertainty of the present $^{233}$U$(n, f)$ cross-section is composed of contributions related to the sample masses, the $^{235}$U$(n, f)$ cross-section, the dead-time and efficiency corrections, the beam energy resolution, and the counting statistics.

The determination of the sample masses by $\alpha$ spectroscopy led to uncertainties of 1.2% and 1.35% for $^{233}$U and $^{235}$U, respectively, which add to a 1.8% contribution for the cross-section. The uncertainty of the $^{235}$U reference cross-section is typically 2% in the energy region of interest for this work. The very small corrections for the detection efficiencies and dead-time effects are estimated to be of the order of 0.5%.

The resulting 3% systematic uncertainty of the $^{233}$U$(n, f)$ cross-section clearly dominates over the statistical component, which is always below 1% if the data are given with a resolution of 20 bins/decade.

The related neutron energies were determined by assuming a common flight path. The uncertainty resulting from the actual 10 mm spacing between the samples is $\approx 0.05\%$ and was, therefore, neglected in view of the energy resolution, which corresponds to an uncertainty of 0.7% at 10 MeV.

### 4 Results

The neutron-induced fission cross-section of $^{233}$U was determined with the ratio method between 0.5 and 20 MeV.

**Table 2.** The $^{233}$U$(n, f)/^{235}$U$(n, f)$ cross-section ratio and the final $^{233}$U$(n, f)$ cross-section in the neutron energy range between 0.5 and 20 MeV and the respective total uncertainties.

| Energy (MeV) | $^{233}$U$(n, f)/^{235}$U$(n, f)$ | $^{233}$U$(n, f)$ (b) |
|---|---|---|
| 0.501–0.562 | $1.76 \pm 0.06$ | $2.00 \pm 0.06$ |
| 0.562–0.631 | $1.72 \pm 0.06$ | $1.92 \pm 0.06$ |
| 0.631–0.708 | $1.74 \pm 0.06$ | $1.94 \pm 0.06$ |
| 0.708–0.794 | $1.72 \pm 0.06$ | $1.92 \pm 0.06$ |
| 0.794–0.891 | $1.68 \pm 0.05$ | $1.87 \pm 0.06$ |
| 0.891–1.000 | $1.58 \pm 0.05$ | $1.86 \pm 0.06$ |
| 1.00–1.12 | $1.54 \pm 0.05$ | $1.84 \pm 0.06$ |
| 1.12–1.26 | $1.54 \pm 0.05$ | $1.84 \pm 0.06$ |
| 1.26–1.41 | $1.57 \pm 0.05$ | $1.90 \pm 0.06$ |
| 1.41–1.58 | $1.55 \pm 0.05$ | $1.91 \pm 0.06$ |
| 1.58–1.78 | $1.56 \pm 0.05$ | $1.95 \pm 0.06$ |
| 1.78–2.00 | $1.54 \pm 0.05$ | $1.95 \pm 0.06$ |
| 2.00–2.24 | $1.55 \pm 0.05$ | $1.98 \pm 0.06$ |
| 2.24–2.51 | $1.52 \pm 0.05$ | $1.92 \pm 0.06$ |
| 2.51–2.82 | $1.54 \pm 0.05$ | $1.91 \pm 0.06$ |
| 2.82–3.16 | $1.56 \pm 0.05$ | $1.88 \pm 0.06$ |
| 3.16–3.55 | $1.57 \pm 0.05$ | $1.84 \pm 0.06$ |
| 3.55–3.98 | $1.53 \pm 0.05$ | $1.74 \pm 0.06$ |
| 3.98–4.47 | $1.57 \pm 0.05$ | $1.76 \pm 0.06$ |
| 4.47–5.01 | $1.53 \pm 0.05$ | $1.67 \pm 0.06$ |
| 5.01–5.62 | $1.52 \pm 0.05$ | $1.60 \pm 0.05$ |
| 5.62–6.31 | $1.57 \pm 0.05$ | $1.71 \pm 0.06$ |
| 6.31–7.08 | $1.50 \pm 0.05$ | $2.14 \pm 0.07$ |
| 7.08–7.94 | $1.34 \pm 0.05$ | $2.27 \pm 0.08$ |
| 7.94–8.91 | $1.30 \pm 0.04$ | $2.31 \pm 0.08$ |
| 8.91–10.00 | $1.33 \pm 0.05$ | $2.35 \pm 0.08$ |
| 10.00–11.22 | $1.30 \pm 0.04$ | $2.25 \pm 0.08$ |
| 11.22–12.59 | $1.38 \pm 0.05$ | $2.40 \pm 0.08$ |
| 12.59–14.13 | $1.24 \pm 0.04$ | $2.42 \pm 0.08$ |
| 14.13–15.85 | $1.20 \pm 0.04$ | $2.50 \pm 0.09$ |
| 15.85–17.78 | $1.17 \pm 0.04$ | $2.39 \pm 0.08$ |
| 17.78–19.95 | $1.24 \pm 0.04$ | $2.40 \pm 0.08$ |

The careful correction of residual experimental effects has led to accurate data with an overall systematic uncertainty of 3%. The reliability of the results in the investigated energy region could be verified by comparison with the cross-sections of ref. [16], which were derived below 1 MeV from the same raw data but using a different method. In the region of overlap, the results were found to agree within 1%.

The $^{233}$U$/^{235}$U ratios and the final cross-section values are listed in table 2 together with the total uncertainties. For the comparison of the present results with previous data and evaluations, integrated cross-sections over the respective energy regions of overlap are summarized in table 3.

### 4.1 Comparison with previous measurements

In most of previous measurements the cross-section ratio $^{233}$U$(n, f)/^{235}$U$(n, f)$ has been determined with the same

**Table 3.** Energy-integrated cross-sections for comparison with previous results and evaluations; the present results are slightly higher than all previous measurements and evaluations.

| Authors | Ref. | Energy range (MeV) | Difference (%) |
|---|---|---|---|
| Meadows | [8] | 1.–9.4 | +2.1 |
| Fursov *et al.* | [10] | 1.–7.4 | +4.3 |
| Carlson and Behrens | [11] | 1.–20. | +6.3 |
| Kanda *et al.* | [7] | 1.–7.0 | +1.3 |
| Lisowski *et al.* | [9] | 1.–20. | +0.8 |
| Shcherbakov *et al.* | [12] | 1.–20. | +1.9 |
| ENDF/B-VII.0 | | 1.–20. | +3.2 |
| ENDF/B-VI.8 | | 1.–20. | +6.1 |
| JENDL-3.3 | | 1.–20. | +3.9 |
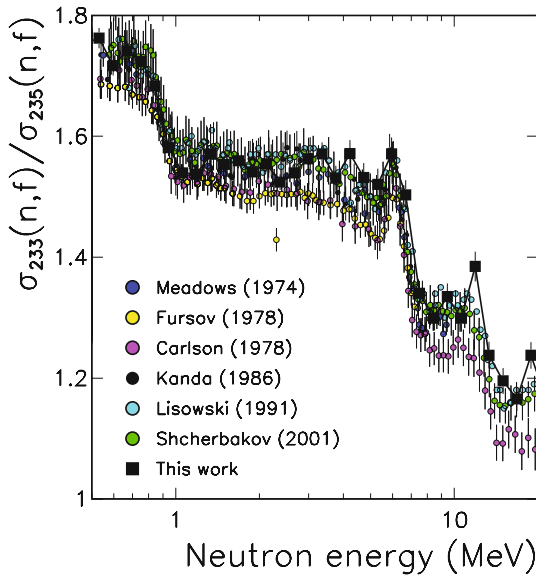


**Fig. 2.** Comparison of the present cross-section ratio $^{233}\mathrm{U}/^{235}\mathrm{U}$ (full squares and solid line, 20 bins per energy decade) with previous measurements [7–12]. For the data reported in ref. [9] information on the related uncertainties is not available.

method as applied in this work. In some cases, also absolute cross-section data are given. A meaningful comparison with the present results can only be made either directly via the cross-section ratios or by deducing the $^{233}\mathrm{U}(n, f)$ cross-section by means of the same $^{235}\mathrm{U}$ standard, thus avoiding systematic effects related to the reference cross-section.

In fig. 2, the results of the present work are compared to the most complete measurements [7–12]. These data exhibit discrepancies around 5%. The present results are in good agreement with Meadows [8] and Kanda *et al.* [7], although these data are limited to neutron energies below 10 MeV. Good agreement is also found with Lisowski *et al.* [9] and Shcherbakov *et al.* [12]. On the contrary, the n_TOF data are $\approx 5\%$ higher than older data of Fursov *et al.* [10] and of Carlson and Behrens [11]. Because the
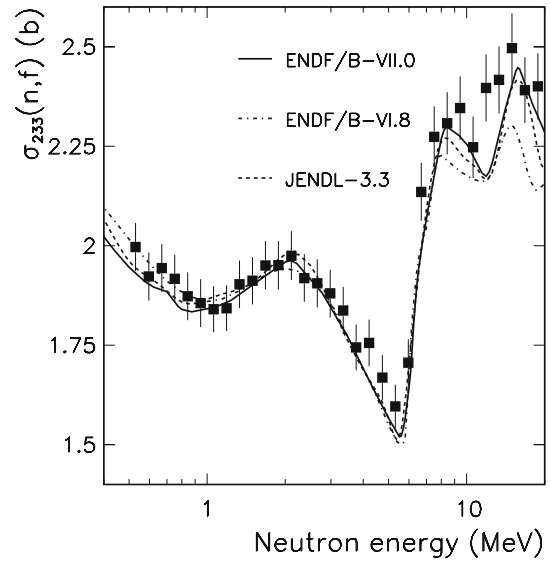


**Fig. 3.** Comparison of present results (full squares, 20 bins/decade) with different evaluations of the $^{233}\mathrm{U}(n, f)$ cross-section [15].

cross-section shapes are in fair agreement in all cases, the differences to previous work can be characterized by the ratios in table 3, which compare the energy-integrated cross-sections over the energy range of the previous measurements. In the limited range of two recent results by Grosjean [13] and Tovesson *et al.* [14] there is agreement within uncertainties.

## 4.2 Comparison with evaluated data

The comparison with current evaluated cross-sections shows reasonable agreement with ENDF/B-VII.0 and JENDL-3.3, where the integrated cross-sections are slightly higher but still compatible within uncertainties as demonstrated in table 3 and fig. 3. The ENDF/B-VII.0 evaluation is mainly based on the data of Kanda *et al.* [7], Meadows [8] and Lisowski *et al.* [9]. It is worth noting that the evaluated cross-section in ENDF/B-VII.0 has been increased in order to reproduce fast critical benchmark experiments.

While good agreement is found between 1 and 8 MeV with all recent evaluations, differences of up to 9% are observed in the energy range between 11 and 15 MeV, just above the threshold for second-chance fission. Given the fact that most previous data do agree with the present results in this energy region, the discrepancy can be attributed to a shortcoming of the evaluations. In addition to the higher cross-section values, the present results suggest also a less pronounced structure in this region.

The file JENDL/AC, specifically devoted to reactor applications, shows a behavior similar to ENDF/B-VII.0, although the fission cross-section of $^{233}\mathrm{U}$ is systematically higher by 1–2%. The JEFF-3.1.1 evaluation and the previous ENDF/B-VI.8 version are in slightly better agreement with the present results below 1 MeV.

# 5 Conclusions

At the n_TOF facility the neutron-induced fission cross-section of $^{233}$U has been measured relative to the fission cross-section standard of $^{235}$U in the energy range between 0.5 and 20 MeV. The two samples were mounted in the same fission chamber and measured simultaneously.

The present results were determined with uncertainties of $\approx 3\%$ due to a minimal $\alpha$-particle background and by careful consideration of all possible sources of systematic uncertainty, in particular related to the efficiency and dead-time corrections.

In general, good agreement is found with most previous measurements, except for some older data. The present data support also recent cross-section evaluations, but below 1 MeV the ENDF/B-VII.0 evaluation underestimates the cross-section, which is better reproduced by the older ENDF/B-VI.8 version. This difference, most probably caused by the impact of an integral measurement, cannot be neglected in view of the importance of this energy range for the design and operation of Th/U-based reactors. A mismatch between the present data and evaluations is also found at the onset of second-chance fission between 11 and 15 MeV. Correspondingly, a slight revision of the evaluations in the energy range from 0.5 to 20 MeV seems to be in order.

# References

1. OECD, International Atomic Energy Agency (IAEA), *URANIUM 2009: Resources, Production and Demand* (OECD Publishing, 2009) see also: `http://www.world-nuclear.org/info/inf75.htm`.
2. *Thorium fuel cycle - potential benefits and challenges*, technical report IAEA-TECDOC-1450 (IAEA, Vienna, 2005) `http://www-pub.iaea.org/MTCD/publications/PDF/TE_1450_web.pdf`.
3. C.D. Bowman *et al.*, Nucl. Instrum. Methods A **320**, 336 (1992).
4. F. Carminati, R. Klapisch, J.P. Revol, Ch. Roche, J.A. Rubio, C. Rubbia, *An energy amplifier for cleaner and inexhaustible nuclear energy production driven by a particle beam accelerator*, technical report CERN/AT/93-47(ET) (CERN, 1993).
5. C. Rubbia *et al.*, *Conceptual design of a fast neutron operated high power energy amplifier*, technical report CERN/AT/95-44(ET) (CERN, 1995).
6. US DOE Nuclear Energy Research Advisory Committee, *A technology roadmap for generation IV nuclear energy systems* (2002).
7. K. Kanda, H. Imaruoka, K. Yoshida, O. Sato, N. Hirakawa, Radiat. Eff. **93**, 233 (1986).
8. J.W. Meadows, Nucl. Sci. Eng. **54**, 317 (1974).
9. P.W. Lisowski, A. Gavron, W.E. Parker, S.J. Balestrini, A.D. Carlson, O.A. Wasson, N.W. Hill, in *Nuclear Data for Science and Technology* (Springer, Jülich, 1991) p. 732.
10. B.I. Fursov, V.M. Kuprijanov, G.N. Smirenkin, At. Energ. **44**, 236 (1978).
11. G.W. Carlson, J.W. Behrens, Nucl. Sci. Eng. **66**, 205 (1978).
12. O.A. Shcherbakov *et al.*, J. Nucl. Sci. Technol. **2**, 230 (2001).
13. C. Grosjean, private communication (2010).
14. F. Tovesson *et al.*, Nucl. Phys. A **733**, 3 (2004).
15. For results compiled in evaluated nuclear data libraries see, for example, the International Atomic Energy Agency (IAEA) `www-nds.iaea.org`, the OECD Nuclear Energy Agency, `www.nea.fr/html/dbdata/`.
16. The n_TOF Collaboration (M. Calviani *et al.*), Phys. Rev. C **80**, 044604 (2009).
17. C. Borcea *et al.*, Nucl. Instrum. Methods A **513**, 524 (2003).
18. The n_TOF Collaboration (U. Abbondanno *et al.*), *CERN n_TOF facility: Performance report*, technical report CERN-SL-2002-053 ECT (CERN, 2003).
19. M. Calviani *et al.*, Nucl. Instrum. Methods A **594**, 220 (2008).
20. The n_TOF Collaboration (U. Abbondanno *et al.*), Nucl. Instrum. Methods A **538**, 692 (2005).
21. The n_TOF Collaboration (G. Lorusso *et al.*), Nucl. Instrum. Methods A **532**, 622 (2004).
22. N. Colonna *et al.*, to be published in Nucl. Instrum. Methods A, (2010).
23. A. Fassò, A. Ferrari, J. Ranft, P.R. Sala, technical report CERN-2005-10 (CERN, 2005).
24. P. Hofmann *et al.*, Phys. Rev. C **49**, 2555 (1994).
25. G.D. Adveev *et al.*, preprint INR 816/93 (1993).
26. A.D. Carlson, V.G. Pronyaev, D.L. Smith, N.M. Larson, Zhenpeng Chen, G.M. Hale, F.-J. Hambsch, E.V. Gai, Soo-Youl Oh, S.A. Badikov, T. Kawano, H.M. Hofmann, H. Vonach, S. Tagesen, Nucl. Data Sheets **110**, 3215 (2009).